Drag anchor fluke–soil interaction in clays

M.P. O'Neill, M.F. Bransby, and M.F. Randolph

Abstract: Finite element analysis has been used to investigate the interaction between anchor flukes and undrained soil at failure. The behaviour of a rectangular and a wedge-shaped anchor has been investigated when the anchors are subject to combined rotational and translational loadings similar to those experienced during anchor dragging. The results have been presented in terms of a plasticity framework to produce an associated plastic failure locus for combined loading conditions. It is seen that the wedge-shaped anchor has a different shaped failure locus and displacements at failure because of its asymmetrical shape, and this will affect drag anchor behaviour. A new design method is introduced that aims to predict drag anchor embedment trajectory and holding capacity through examination of the fluke–soil interaction. The yield loci and plastic potentials produced from consideration of fluke–soil interaction are used in the new design method to predict drag anchor kinematics. Results from the new analysis method are compared to empirically based methods, and it is seen that there is good agreement between results, even without further calibration from physical modelling. This suggests that the approach has promise, and with further refinement of the yield loci and better approximations to the complex anchor geometry, it may develop into a useful anchor design tool that allows for both the anchor geometry and the soil conditions explicitly.

Key words: drag anchor capacity, undrained clays, numerical method.

Résumé : Une analyse en éléments finis a été utilisée pour étudier l'interaction entre les pattes d'ancrage et le sol non drainé à la rupture. Le comportement d'un ancrage rectangulaire et en forme de coin a été étudié dans les conditions où les ancrages sont soumis à des chargements en rotation ou en translation semblables à ceux subis lorsque l'ancrage chasse. Les résultats ont été présentés en fonction d'un cadre de plasticité pour produire une surface de rupture plastique associée pour des conditions combinées de chargement. On voit que l'ancrage en forme de coin a une surface de rupture de forme différente et des déplacements à la rupture différents à cause de sa forme asymétrique, et ceci va influencer le comportement de l'ancrage en chasse. On introduit une nouvelle méthode qui vise à prédire la trajectoire de chasse de l'ancrage enfoui et la capacité de rétention en partant de l'examen de l'interaction patte–sol. Les points de limite élastique et des potentiels plastiques obtenus en partant de la considération de l'interaction patte–sol sont utilisés dans la nouvelle méthode pour prédire la cinématique de la chasse de l'ancrage. On compare les résultats de la nouvelle méthode d'analyse à ceux des méthodes basées sur l'expérimentation, et l'on voit qu'il y a une assez bonne concordance entre les résultats, même sans calibrage supplémentaire en partant du modèle physique. Ceci suggère que cette approche est prometteuse, et qu'avec des raffinements supplémentaires des surfaces limites et avec de meilleures approximations de la géométrie complexe de l'ancrage, elle peut devenir un outil utile de conception d'ancrage qui tient compte de façon explicite tant de la géométrie de l'ancrage que des conditions de sols.

Mots clés : capacité de rétention d'ancrage, argiles non drainées, méthode numérique.

[Traduit par la Rédaction]

Introduction

The recent trend of new offshore developments to move into deeper waters has resulted in a greater reliance on anchored floating structures, as opposed to traditional fixed-jacket or gravity-based structures. Furthermore, these structures are often required to be anchored in soft, normally consolidated, or slightly overconsolidated clays and silts. The drag anchor and chain system is one common mooring system that is used to tether floating structures to the seabed. Historically, the design of drag anchors has been empirically based (Vryhof Anchors 1990), but more recent approaches (Neubecker and Randolph 1996; Thorne 1998; Dahlberg 1998) have been proposed that predict the entire drag trajectory and holding capacity of an anchor in clay. These approaches are based on limit equilibrium analyses that use basic geomechanics principles to identify the geotechnical loads acting on the anchor and kinematic analyses that use simple assumptions regarding the movement of the anchor. There still remains a limited degree of empiricism within these solutions (e.g., the anchor form factor, f, Neubecker and Randolph 1996), and therefore a need exists for more rigorous prediction methods using fundamental soil mechanics principles.

As a drag anchor approaches its ultimate holding capacity (UHC) in soft undrained soils, failure of the soil can be

Received 12 October 2001. Accepted 6 August 2002. Published on the NRC Research Press Web site at http://cgj.nrc.ca on 21 January 2003.

M.P. O'Neill and M.F. Randolph. Centre for Offshore Foundation Systems, University of Western Australia, 35 Stirling Highway, Crawley WA 6009, Australia.
M.F. Bransby.[1] Division of Civil Engineering, University of Dundee, Dundee DD1 4HN, U.K.

[1]Corresponding author (e-mail: m.f.bransby@dundee.ac.uk).

 doi: 10.1139/T02-096 © 2003 NRC Canada

assumed to consist of localized plastic flow around the anchor fluke and shank. The behaviour of the anchor will be largely independent of the orientation of the anchor with respect to the soil surface, and therefore detailed analysis of the soil surrounding the fluke will provide valuable insight regarding the general behaviour of anchors in clay.

This paper presents the results of an investigation of the soil around the anchor flukes of two different shapes using finite element (FE) analyses. The resulting behaviour has been characterized in terms of plastic yield envelopes, which in turn permits the investigation of anchor behaviour under general catenary loading conditions. The results are compared to existing design methods, and it is hoped that the method will ultimately lead to novel numerical anchor design tools using the yield envelope approach.

Review of numerical studies for plate anchors in clay

Over the last three decades, the majority of the studies concerning the uplift behaviour of anchor plates in clay have been based on simple analytical solutions or experimental data. Relatively few have been conducted using numerical analyses; the most rigorous of these was performed by Rowe and Davis (1982). In their paper, elastic-plastic FE analyses were used to derive results describing the behaviour of vertical and horizontal strip anchors embedded in uniform clay. Included in the investigation were studies concerning the effect of anchor roughness, embedment depth, anchor thickness, and anchor shape.

Merifield et al. (2001) performed similar studies into the stability of vertical and horizontal strip footings embedded in clay. Bounds on the ultimate pullout capacity were obtained by employing numerical procedures based on FE formulations of the upper and lower bound theorems of limit analysis. These formulations assumed a perfectly plastic clay model with a Tresca yield criterion. Various aspects were examined, including the strength profile of the soil and the footing geometry.

Colwill (1996) conducted two- and three-dimensional FE analyses of the pullout of plate anchors in clay. The analyses accounted for variations in the embedment ratio (embedment depth divided by the plate length), the inclination of the plate, and the inclination of the line of pull, although the results appeared to contain numerical errors. Bearing capacity factors generated by these analyses were implemented into a simulation model titled *ASM-Clay*, enabling the prediction of drag anchor behaviour in undrained soils. The output from the model was shown to agree well with the results of model anchor tests performed in the centrifuge.

Plasticity concepts

The bearing capacity of a shallow foundation undergoing combined vertical, V, horizontal, H, and moment, M, loading has been a problem of great interest to soil mechanics researchers for many years. More recently, the focus has centered on the analysis of offshore foundations under combined loading, employing plasticity concepts and yield loci in V-H-M space. Experimental and theoretical modelling of spudcan behaviour under combined loading was performed by Tan (1990) and Martin (1994) in drained or partially drained sand and clay, respectively. Bransby and Randolph (1998) studied the combined loading response of skirted foundations in cohesive soil using FE analysis and upper bound plasticity analysis.

The plastic yield locus of a particular foundation expresses the combination of V, H, and M loads that result in failure of the given foundation. For a given geometry and set of soil conditions, the locus can be expressed as a mathematical function of V, H, and M

$$[1] \qquad f(V,H,M) = 0$$

This function can be illustrated graphically. A typical yield locus, plotted in H-V space with $M = 0$ is shown in Fig. 1*a* and describes the combination of horizontal and vertical loads that will result in the failure of a typical embedded footing of characteristic length, L_f, and depth, d_f, as illustrated in Fig. 1*b*. For this locus, the maximum vertical and horizontal resistance loads, V_{max} and H_{max}, occur when H and V, respectively, are equal to zero.

As well as enabling the calculation of foundation capacity under combined loads, the yield locus may also form a plastic potential, allowing determination of the relative values of the plastic vertical, δv, horizontal, δh, and rotational, $\delta\beta$, displacements of the foundation at failure. Chen (1975) demonstrated that if the soil surrounding an element obeyed the condition of normality (i.e., plastic flow with no change in volume), then normality would also apply for an overall foundation yield locus. This was confirmed by Bransby and Randolph (1998) using FE analysis to investigate the combined loading response of skirted foundations. A similar approach has been adopted for analyzing multifooting offshore structures such as mobile drilling rigs (Murff 1994; Martin and Houlsby 2001). Hence, the condition of normality or associated flow, whereby the gradient of the yield locus defines the ratio of plastic displacements at failure, holds for undrained failure conditions when the soil remains attached to the foundation. It follows that for the embedded footing illustrated in Fig. 1*b*, the associated yield locus presented in Fig. 1*a* can be used to determine the relative magnitudes of the resulting plastic horizontal and vertical displacements, δh and δv, respectively, at failure.

The application of plasticity analysis to anchors

Consider a simplified weightless drag anchor deeply embedded in undrained soil, as illustrated in Fig. 2. Temporarily ignoring the contribution of the shank, a chain load, T_a, exerted on the anchor pad eye can be expressed in terms of forces parallel (H) and perpendicular (V) to the top face of the fluke and (negative) moment (M) about a particular reference point on the fluke. Combinations of these three loads (H, V, and M) will result in failure of the anchor and anchor movements parallel (δh) and perpendicular (δv) to the fluke and rotationally ($\delta\beta$) about the same fluke reference point. During anchor penetration, the fluke will rotate in the direction defined as giving a positive $\delta\beta$ and so the sign convention for M is given as shown in Fig. 2.

Since the anchor is assumed to be deeply embedded, failure of the soil will be fully constrained and local to the anchor fluke regardless of the direction of the load. This implies that the failure loads H, V, and M will be independent of anchor orientation. Therefore, the local loads at the fluke reference point defined in Fig. 2 can be assumed to be appropriate for all fluke failure conditions. Furthermore, the

© 2003 NRC Canada

Fig. 1. The yield locus and plastic potential function.

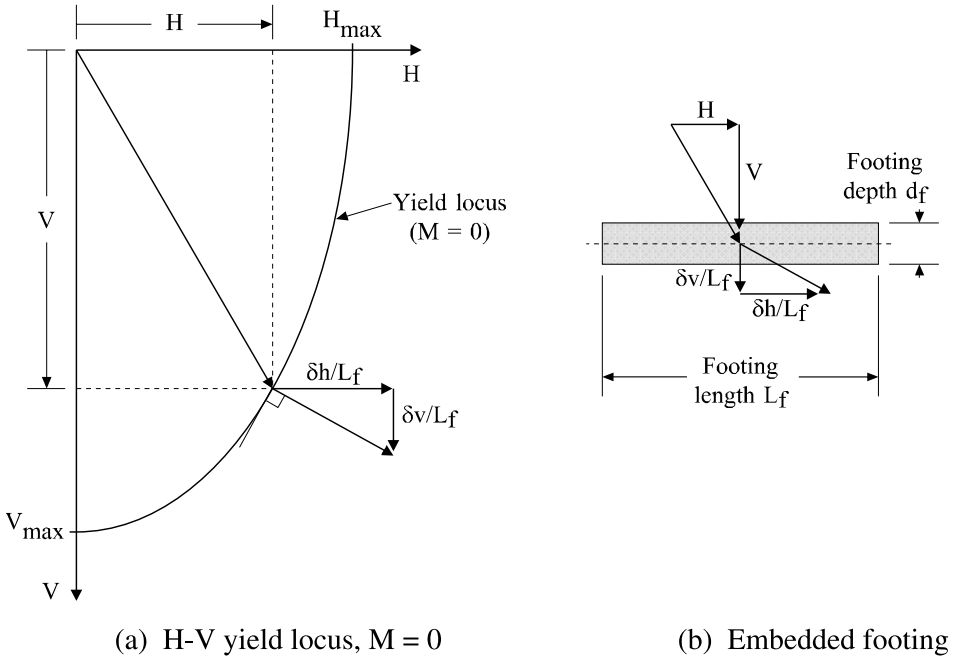

Fig. 2. Loads and displacements at failure for a simplified drag anchor.

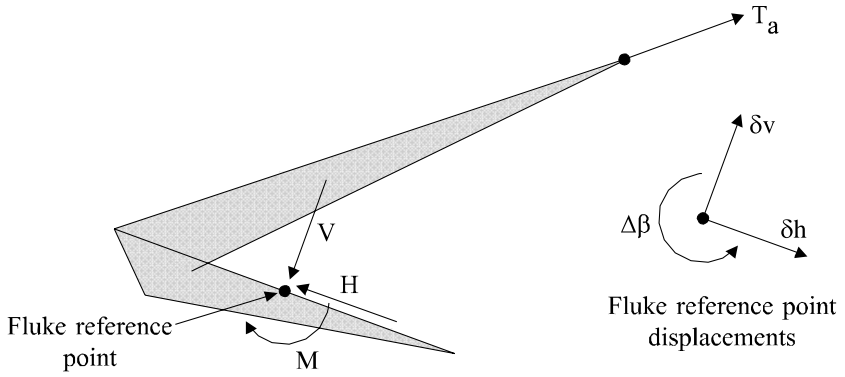

deep condition ensures that the soil remains attached to the fluke, and hence plastic fluke displacements will be governed by normality to the failure locus, $f(H,V,M)$. In simpler terms, determination of the fluke yield locus will enable prediction of the direction of fluke displacement at failure. It should be noted that this approach assumes that elastic displacements are negligible when compared to the plastic displacements, but this is very likely at a state of continual failure.

Owing to the relatively complex geometry of modern drag anchors, the anchor failure loads (H, V, and M) will be the result of very complicated three-dimensional (3D) soil displacements. A detailed investigation of these displacements would require a full 3D analysis, incorporating the complete 3D geometry of the anchor. This would be extremely time-consuming, computationally expensive, and anchor specific. Furthermore, it is believed that many of the complexities of drag anchor behaviour may be understood by closely examining the anchor fluke alone. This approach stems from the widely accepted assumption that the fluke provides a large proportion of the anchor's holding capacity and governs much of the anchor's kinematics.

Therefore, the scope of this investigation using FE analysis only encompasses fluke–soil interaction in clay, and the results of the analysis are expressed as plastic yield loci. These are then used to make predictions of anchor trajectory and holding capacity. The main thrust of the work is to demonstrate a new approach for predicting drag anchor trajectory and holding capacity from knowledge of the anchor geometry and soil conditions. In the first instance, the FE analyses have assumed homogeneous soil conditions, and for application to nonhomogeneous conditions, the resulting yield envelopes are assumed to be scaled to the average soil strength at the current fluke position. This is clearly a simplification, and refinement will be needed in the future to accommodate specific anchor shapes and to take account of variations of soil strength with depth in a more rigorous fashion.

Finite element analysis

Geometry and soil model

The general aim of the FE analyses was to examine fluke–soil interaction behaviour during deep, undrained failure

© 2003 NRC Canada

Fig. 3. Simplified fluke geometry and definitions.

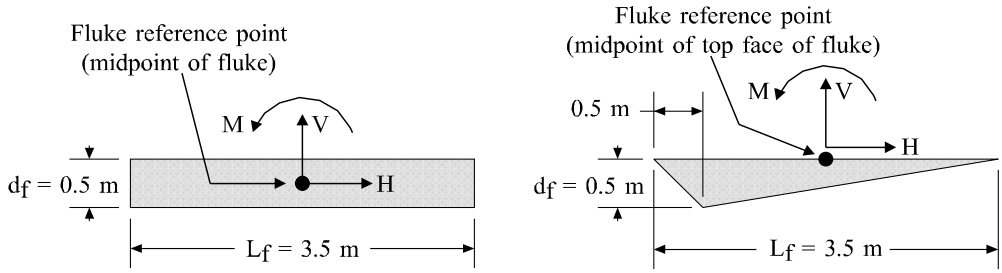

(a) Rectangular fluke (b) Wedge fluke

conditions and, more specifically, to deduce the shape and nature of the *H-V-M* yield loci for flukes of different shapes. To allow plane strain analysis, the fluke shapes were idealized as being infinitely wide. Although this may be seen as a crude approximation to real 3D flukes, it does permit detailed analysis of simpler geometries, which may enable a clearer understanding of the fluke–soil interaction problem.

Two simple fluke cross-sections were adopted for the analyses, these being a rectangular fluke and an eccentric wedge fluke. The dimensions of the flukes are defined in Fig. 3. A length over depth ratio $L_f/d_f = 7$ was adopted for both flukes, as this is similar to that of a Vryhof Stevpris anchor fluke (Vryhof Anchors 1990). Furthermore, the front and back wedge angles of 45.0 and 9.5°, respectively, for the wedge fluke are also similar to those of a Stevpris fluke. The reference point for the rectangular fluke was taken as the overall fluke midpoint, while for simplicity the reference point of the wedge fluke was taken as the midpoint of the top fluke face. The reference point must be fixed for the analysis of the wedge and the anchor kinematics. The location of the reference point will affect the shape of the yield locus but not the results of the anchor system analysis, and so its choice is arbitrary.

The FE package CRISP (CRItical State Program) was used for all analyses (Britto and Gunn 1987). The rectangular fluke mesh consisted of approximately 850 cubic strain triangular elements with 16 degrees of freedom (Sloan and Randolph 1982). A diagram of the overall mesh is presented in Fig. 4*a*, and a close-up diagram of the central area of the mesh around the rectangular fluke is shown in Fig. 4*b*. To simulate deep conditions, all four outer mesh boundaries were fixed in the horizontal and vertical directions. The mesh used in the analysis of the wedge fluke was similar, but contained approximately 200 additional elements. A close-up of the central area of the mesh around the wedge fluke is shown in Fig. 4*c*. Problems associated with the singularities at the corners of the wedges were minimized by using a high density of mesh, and as shown later, the analyses for the simple loading cases (for example *V* only) gave close agreement with the results from the upper bound solutions, demonstrating the adequacy of the mesh. Both flukes were assumed to be rigid and fully rough, so that no interface elements were necessary.

The soil was modelled as a uniform, weightless, elastic-plastic Tresca material with a rigidity index, $G/s_u = 500$. Furthermore, the soil was modelled as undrained by the use of total stress analysis, together with a Poisson's ratio, $\nu = 0.49$. It should be noted that the results of the analysis are relatively insensitive to the shear stiffness of the soil. For vertical (normal to fluke) and moment (rotational) failure, the mechanisms involve local constrained shear failure, and the limit loads are unaffected by prefailure shear stiffness (Chen 1975). For the horizontal (parallel to fluke) failure, there will be a minor affect of shear stiffness owing to the bearing capacity failure mode at the leading and trailing edges of the fluke (see later discussion of Fig. 8). However, this will have limited effect on the overall yield envelope. This soil model is therefore considered an appropriate approximation for the investigation of plastic yield or failure loci, but further refinement would be required for investigations of behaviour prior to failure.

Displacement-controlled analyses were adopted, since they are more suitable for determining yield loci than load-controlled analyses (Bransby and Randolph 1997). In each analysis, the fluke was slowly displaced at the fluke reference point in a particular displacement direction, such that $\delta v/\delta\beta$ and $\delta h/\delta\beta$ were constant. Displacement of the fluke proceeded until a plastic failure load was attained. After performing a series of these displacement probes with different $\delta v/\delta\beta$ and $\delta h/\delta\beta$ ratios, the final *H*, *V*, and *M* load points were used to characterize the full yield locus of the fluke.

Rectangular fluke analysis results

Typical load–displacement curves for a rectangular fluke displacement probe are featured in Fig. 5. In this particular analysis, the fluke was displaced at 30° to the horizontal with zero rotation (i.e., $\delta v/\delta h = 0.577$, $\delta\beta = 0$). The curves show the vertical, *V*, and horizontal, *H*, load response of the fluke, normalized by the fluke length, L_f and the undrained shear strength, s_u, plotted against the normalized fluke reference point displacement, s_f/L_f (where $s_f = (\delta v^2 + \delta h^2)^{0.5}$). For both curves, the load response is shown to be relatively stable, with the respective failure loads being attained within a fluke displacement of 2% of the fluke length (i.e., $(s_f/L_f)/(s_u/G) = 10$).

Figure 6 shows the final load points from a series of rectangular fluke displacement probes performed using different combinations of horizontal, *h*, and vertical, *v*, translation. The horizontal and vertical loads are again presented in dimensionless $H/(L_f s_u) - V/(L_f s_u)$ space. The results indicate that there is a convex yield locus as required from plasticity theory (Chen 1975). Pure vertical translation resulted in a maximum vertical load capacity, $V_{max}/(L_f s_u) = 11.87$, with *H* and *M* equal to zero. Likewise, pure horizontal translation resulted in a maximum horizontal load capacity, $H_{max}/(L_f s_u) = 4.29$, with *V* and *M* equal to zero. As the ratio of vertical to

© 2003 NRC Canada

Fig. 4. Finite element meshes.

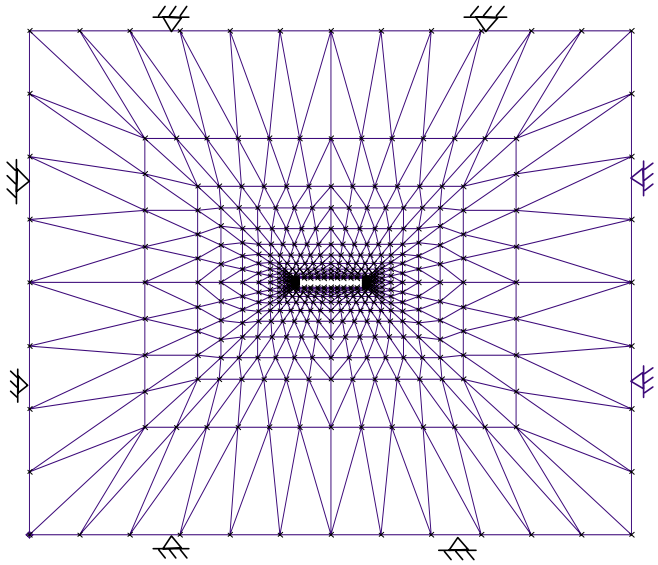

(a) Complete rectangular fluke mesh

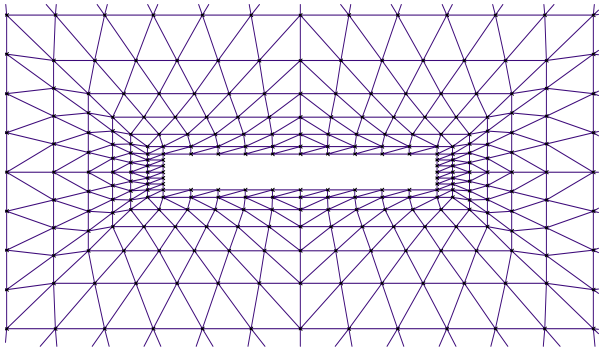

(b) Close-up of rectangular fluke mesh

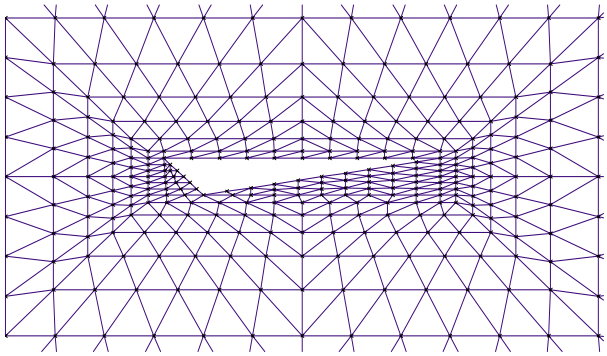

(c) Close-up of wedge fluke mesh

Fig. 5. Load–displacement response obtained from FE analysis for rectangular fluke displaced at 30° to horizontal only ($\delta v/\delta h$ = 0.577, $\Delta\beta$ = 0).

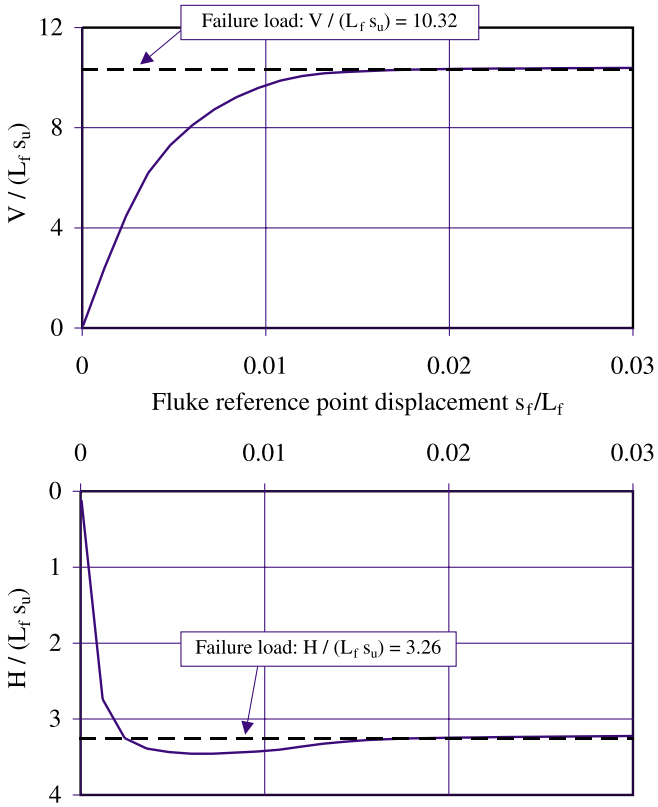

Fig. 6. Rectangular fluke yield locus in *V-H* space.

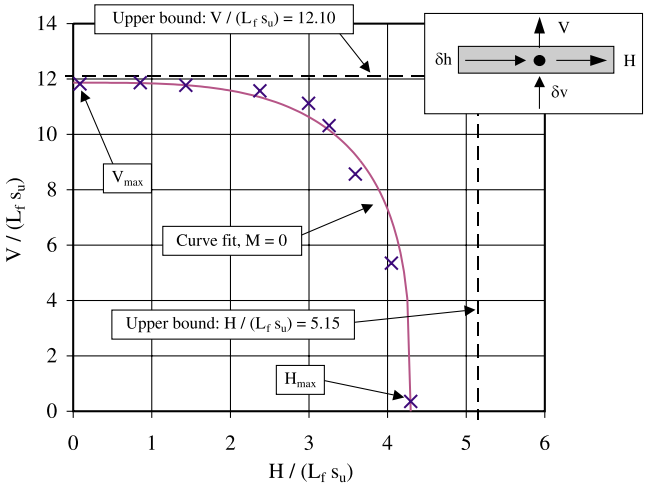

horizontal ($\delta v/\delta h$) displacement increased, there was a sharp increase in vertical resistance, accompanied by a gradual decrease in horizontal resistance. Note that the curve-fitted yield locus corresponding to $M = 0$ and featured in Fig. 6 is calculated using a procedure outlined in the section titled "Curve fitting of the yield loci".

The peak horizontal and vertical loads, H_{max} and V_{max}, for the rectangular fluke can be compared to solutions obtained using upper bound plasticity calculations. Proposed kinematic failure mechanisms for the upper bound calculation of V_{max} and H_{max} are featured in Figs. 7*a* and 8*a*, respectively. Both mechanisms feature single soil wedges on the fluke faces perpendicular to the direction of displacement. Taking α as the angle subtended by the failure wedge and the fluke surface, the upper bound calculations give

$$[2] \qquad \frac{V_{max}}{L_f s_u} = 4\left(\pi - \alpha + \frac{\tan\alpha}{2}\right) + 4\frac{d_f}{L_f}\left(\frac{1}{2} + \cos\alpha\right)$$

© 2003 NRC Canada

Fig. 7. Upper bound mechanisms and FE-calculated soil displacements for rectangular fluke at V_{max}.

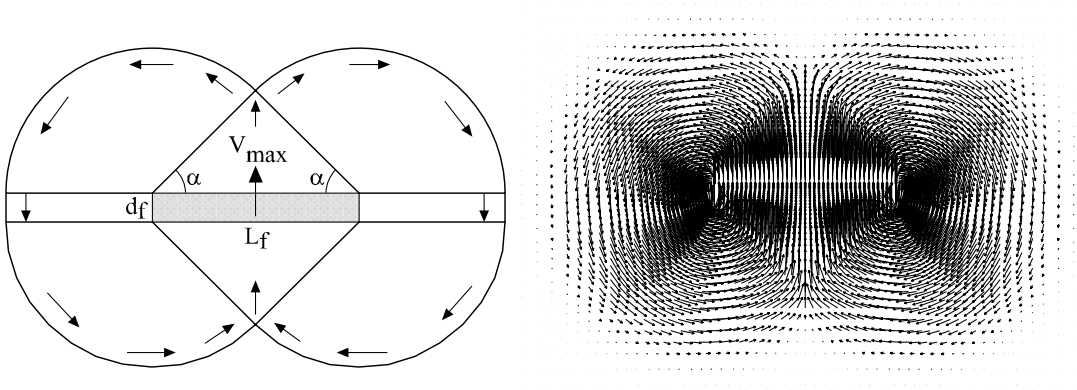

(a) Upper bound mechanism (b) FE calculated soil displacements

Fig. 8. Upper bound mechanisms and FE-calculated soil displacements for rectangular fluke at H_{max}.

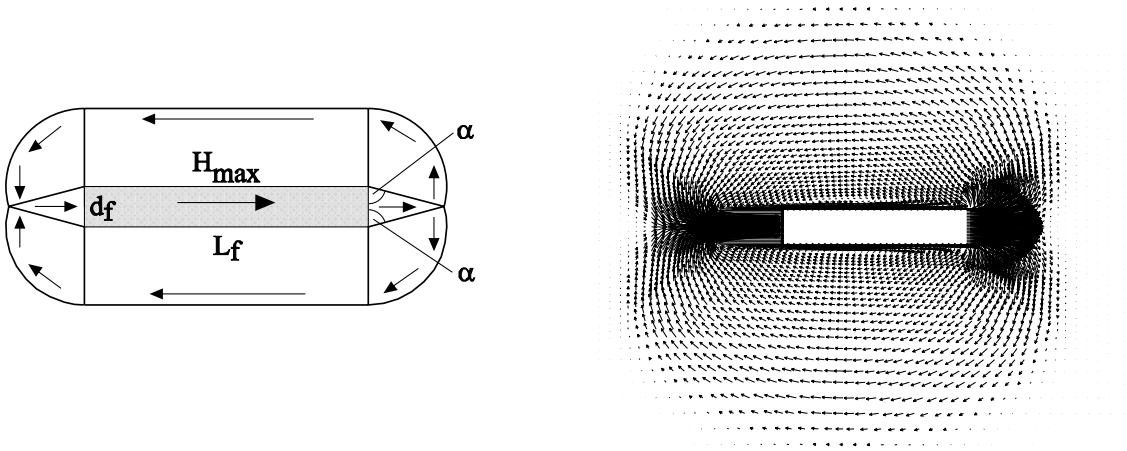

(a) Upper bound mechanism (b) FE calculated soil displacements

$$[3] \qquad \frac{H_{max}}{L_f s_u} = 4\frac{d_f}{L_f}\left(\pi - \alpha + \frac{\tan\alpha}{2}\right) + 4\left(\frac{1}{2} + \cos\alpha\right)$$

Varying α results in minimum values of $V_{max}/(L_f s_u)$ = 12.10 (α = 47.7°) and $H_{max}/(L_f s_u)$ = 5.15 (α = 75.3°).

The upper bound predictions of V_{max} and H_{max} for the rectangular fluke are included in Fig. 6 for comparison with the FE results. The two separate calculations of V_{max} show excellent agreement, with the upper bound result exceeding the FE result by only 2%. However, the calculations for H_{max} do not exhibit the same level of agreement, with the upper bound result exceeding the FE result by 20%.

The soil deformation mechanisms in the FE calculations at V_{max} and H_{max} for the rectangular fluke are shown in Figs. 7*b* and 8*b*, respectively. Examination of the mechanism for V_{max} shows that it is very similar to the mechanism adopted in the upper bound calculation, and it supports the good agreement between the results. However, there is a significant difference between the FE-calculated mechanism and the upper bound mechanism for H_{max}, explaining the disparity between the calculated values of H_{max}. Interestingly, a simple calculation assuming a plane strain bearing capacity factor of 7.5 on the vertical (end) fluke faces and full development of the undrained shear strength along the horizontal (top and bottom) fluke faces gives a value of $H_{max}/(L_f s_u)$ = 4.14, which is approximately 3% less than the FE-calculated value.

Pure rotation of the rectangular fluke about the fluke reference point, with zero horizontal and vertical translation, resulted in the dimensionless FE-calculated maximum moment capacity, $M_{max}/(L_f^2 s_u)$ = 1.49. An upper bound calculation for M_{max}, utilizing a rotational scoop mechanism as shown in Fig. 9*a*, results in the general expression

$$[4] \qquad \frac{M_{max}}{L_f^2 s_u} = \frac{\pi}{2}\left[1 + \left(\frac{d_f}{L_f}\right)^2\right]$$

Solution of this upper bound expression gives $M_{max}/(L_f^2 s_u)$ = 1.60, which is only 7% greater than the FE-calculated value. This good agreement in the calculated values of M_{max} is explained by the similarity of the upper bound mechanism with the FE-determined soil displacement mechanism featured in Fig. 9*b*, and it suggests that the FE analysis is numerically stable.

The complete rectangular fluke yield locus is outlined in Fig. 10 and illustrates the final load points from the full set

© 2003 NRC Canada

Fig. 9. Upper bound mechanism and FE-calculated soil displacements for rectangular fluke at M_{max}.

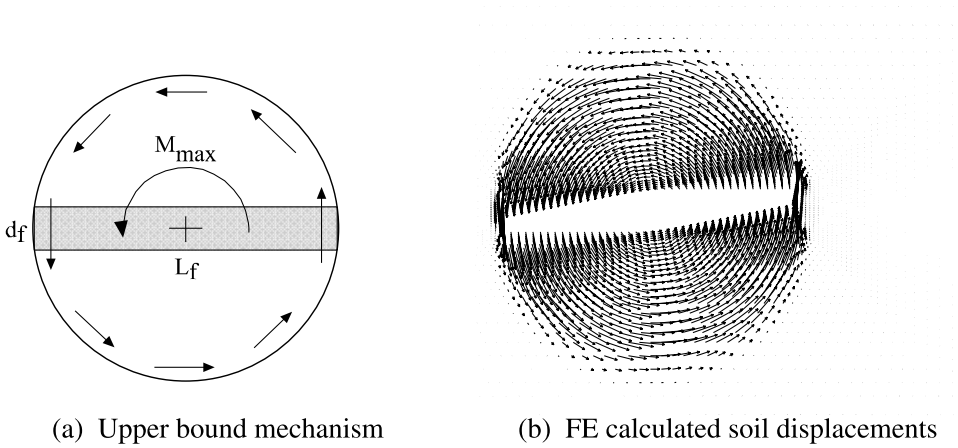

(a) Upper bound mechanism (b) FE calculated soil displacements

Fig. 10. *H-V-M* yield locus for rectangular fluke.

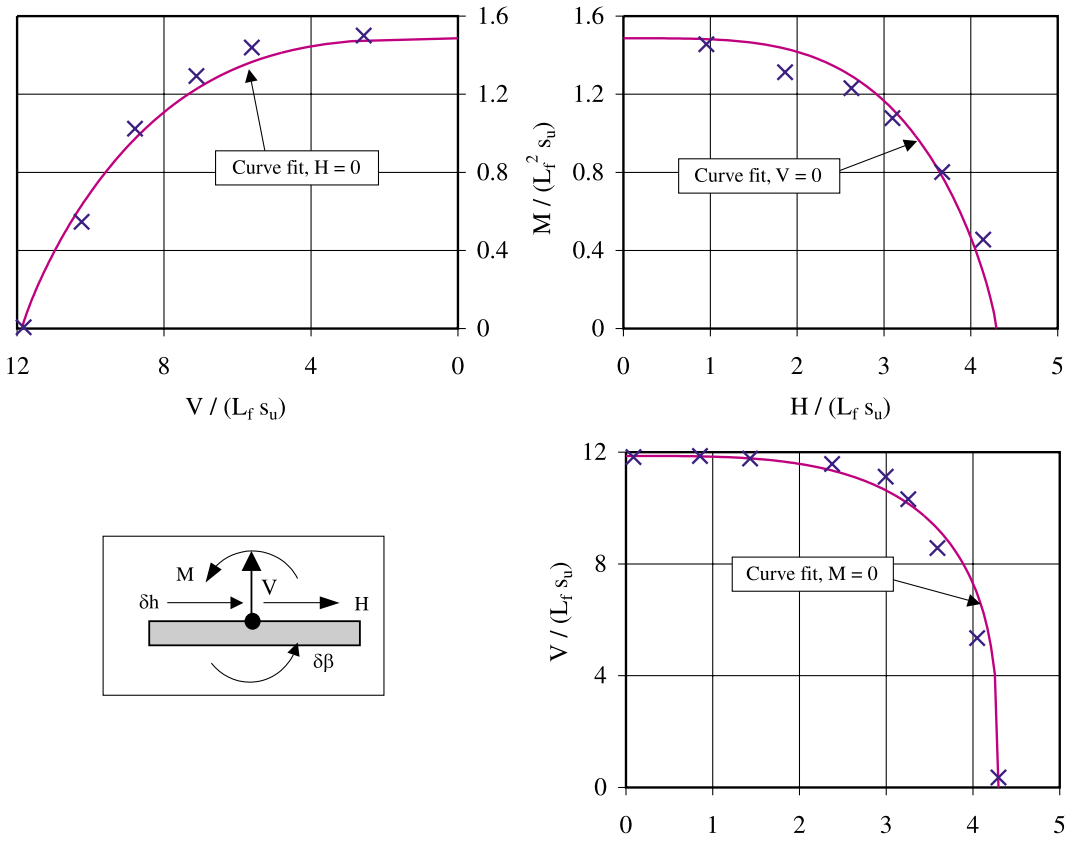

of FE analyses plotted in nondimensional *M-H*, *M-V*, and *V-H* space. The load points show the locus to be convex and symmetrical about the *H-M-V* axes. Note that the curve-fitted yield loci featured in Fig. 10 are calculated using a procedure outlined in the section titled "Curve fitting of the yield loci".

Wedge fluke analysis results

Figure 11 presents the yield locus eventuating from the full set of wedge fluke displacement probes performed using different combinations of horizontal, δh, vertical, δv, and rotational, $\delta\beta$, displacement. The final load points are plotted in dimensionless *M-H*, *M-V*, and *V-H* space, in each case taking a slice through the yield envelope at the offset value of the third load component (V_1, H_1, and M_1, respectively), as explained in the section titled "Curve fitting of the yield loci". The value of $V_{max}/(L_f\ s_u) = 11.53$ for the wedge fluke compares well with the associated value for the rectangular fluke, owing to the relatively similar profiles of the different flukes normal to the horizontal fluke axis. The maximum nondimensional moment load of $M_{max}/(L_f^2\ s_u) = 1.60$ for the wedge fluke also compares favourably with the corresponding rectangular fluke value. By contrast, the value of $H_{max}/(L_f\ s_u) = 3.34$ for the wedge fluke is somewhat lower

© 2003 NRC Canada

Fig. 11. *H-V-M* yield locus for wedge fluke.

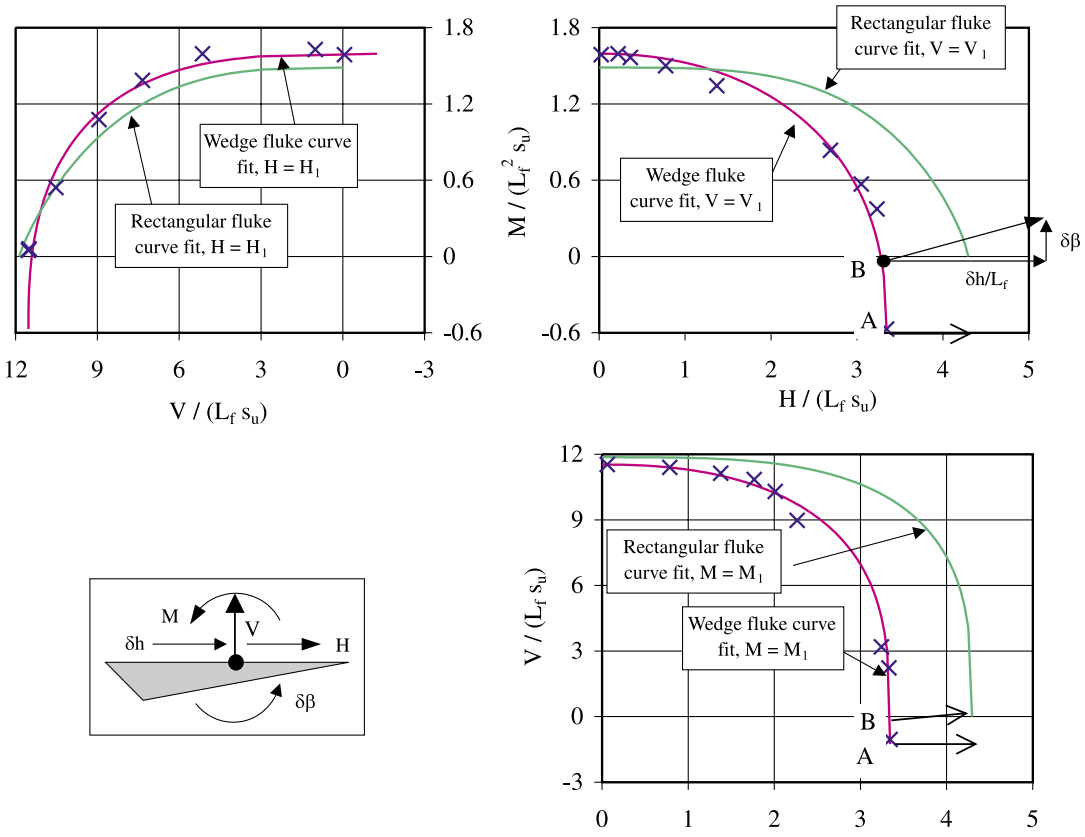

than the corresponding value for the rectangular fluke, due primarily to the wedge's inclined front face.

In their numerical study into wedge penetration in clay, Baligh and Scott (1976) examined the force required to produce steady-state motion of a rigid wedge of varying wedge angle through a rigid perfectly plastic material. It was found that for a fully rough wedge with a wedge angle of 9.5° corresponding to the fluke wedge angle, the resulting horizontal bearing factor, $H/(d_f s_u)$, was equal to 18.03, where d_f was the wedge depth, and s_u was the yield shear strength of the soil. The corresponding value suggested by the curve-fitted wedge fluke yield locus, assuming that the fluke is displaced parallel to the fluke middle axis (i.e., $\tan^{-1}(\delta v/\delta h) = 4.75°$), is $H/(d_f s_u) = 22.47$. This is slightly higher than the Baligh–Scott value, but it is worth noting that the Baligh–Scott solution assumed the formation of a gap behind the wedge, whereas the fluke wedge analysis presented here assumed that the soil remained attached to the fluke. Indeed, detachment of the soil behind the wedge in the Baligh–Scott mechanism would lead to a slightly reduced net horizontal resistance compared to the current analyses.

More importantly, the wedge fluke yield locus, represented by the load points in Fig. 11, differs substantially from that for the rectangular fluke, featured in Fig. 10, in that it is asymmetric. For example, under pure horizontal translation, where $\delta h > 0$ and $\delta v = \delta\beta = 0$, H_{max} will be sustained along with negative V and negative M (point A in Fig. 11). An alternative way of examining the same effect is that if the wedge fluke was released vertically and rotationally, and was loaded horizontally (positive δh or to the right) to failure at point B in Fig. 11, the fluke would also be forced by the soil to move upwards (positive δv) and rotate anticlockwise (positive $\delta\beta$). Interestingly, this suggests that under pure horizontal load the wedge fluke moves along a plane lying approximately parallel to the bottom fluke face. This shift in the yield locus, when compared to the rectangular fluke, highlights the asymmetric and complex kinematics of the wedge fluke.

Curve fitting of the yield loci

The yield loci defined by the endpoints of the FE analyses may be fitted by a single mathematical function in *H-V-M* space. Preliminary curve fitting has indicated that an offset form of the Murff (1994) equation gives the best fit to the analysis results

$$[5] \quad f = \left(\frac{V - V_1}{V_{max} - V_1}\right)^q - 1 + \left[\left(\frac{M - M_1}{M_{max} - M_1}\right)^m + \left(\frac{H - H_1}{H_{max} - H_1}\right)^n\right]^{\frac{1}{p}}$$

The maximum load values V_{max}, M_{max}, and H_{max}, along with the offset load values V_1, M_1, and H_1, are obtained from the FE analyses. The exponents m, n, p, and q are determined via a least squares regression scheme to obtain a best-fit solution. Table 1 summarizes the resulting values of these parameters for the rectangular and wedge fluke yield loci.

© 2003 NRC Canada

Table 1. Yield loci curve-fitting parameters.

Parameter	Rectangular fluke	Wedge fluke
$H_{max}/(L_f s_u)$	4.29	3.34
$V_{max}/(L_f s_u)$	11.87	11.53
$M_{max}/(L_f^2 s_u)$	1.49	1.60
$H_1/(L_f s_u)$	0	0
$V_1/(L_f s_u)$	0	–1.25
$M_1/(L_f^2 s_u)$	0	–0.57
m	1.26	2.37
n	3.72	2.14
p	1.09	0.93
q	3.16	3.41

The fitted curves representing the yield locus for the rectangular and wedge flukes are shown in Figs. 10 and 11, respectively, plotted with the final FE-determined load points. For direct comparison, Fig. 11 features the curve-fitted yield loci for both the rectangular and wedge flukes. In each two-dimensional (2D) load space, the curve is presented with the third load dimension equal to the related offset value (e.g., M_1 for the *V-H* load space). For the symmetrical rectangular fluke yield locus, these offset values are equal to zero. Comparison with the final load points from the respective FE analyses shows that the fitted curves give reasonably good agreement.

There appears to be a sudden change in gradient of the yield locus in *H-V* space. An example of this is illustrated in Fig. 6 (rectangular fluke) at $H/(L_f s_u) = 3.0$ and $V/(L_f s_u) \approx 11.0$, where a yield locus curve fit in two parts on either side of this point would potentially provide a closer fit to the numerical results. This would require additional analyses close to the singularity point and more detailed investigations of the related mechanisms.

For the purposes of anchor design and analysis, the combined loading conditions near H_{max} are of greatest interest. Additional analyses and more complex curve fitting to allow for the detailed shape of the yield locus in this region may be required.

Kinematic anchor analysis

Outline

The yield loci curve fits to the FE analyses can be used in the kinematic analysis of drag anchors in cohesive soil. This new approach is similar to that proposed by Neubecker and Randolph (1996) with the major difference being the use of plasticity concepts to determine the forces acting on the fluke in the equilibrium solution and the use of the associated plastic anchor displacements to determine the anchor kinematics. A flowchart outlining the procedure of this approach is presented in Fig. 12, while a more detailed outline of the procedure is provided in the following sections. Note that a key assumption is that, as the anchor advances through the soil, the resistance mobilized is the steady state value attributable to the local (average) shear strength of the soil for the current fluke position.

Simplification of the anchor-chain system

The geometry of the drag anchor to be modelled is illustrated in Fig. 13. The idealized fluke of length L_f, depth d_f, and width b_f, is assumed to be wide enough such that it can be idealized as acting in plane strain. The shank is modelled as a single flat plate of length L_s, width b_s (into the page), and inclined to the top face of the fluke at the fluke-shank angle, θ_{fs}. Note that, in reality, the shank consists of a pair of relatively narrow plates (side by side into the page) and much of the soil resistance on the shank consists of sliding over those plates. The width, b_s, adopted here has been judged to offer similar overall resistance to forward motion of the shank. The effect of soil resistance over the shank on the yield envelope of the fluke has been ignored here; this is considered reasonable for anchors in clay where soil can flow relatively freely through the structural components of the shank.

The anchor-chain system is idealized as illustrated in Fig. 13. The soil is assumed to have a surface undrained shear strength s_{uo}, and an undrained shear strength gradient with depth, s_{ug}. The anchor pad eye is at an embedment depth, d_a, below the soil surface, and the top face of the fluke is inclined at an angle, β, to the horizontal. The anchor chain of effective width, b_c, is connected to the pad eye at an inclination to the horizontal, θ_a, and under a tension, T_a.

Although the FE analyses used in the determination of the fluke yield loci were performed assuming a constant undrained shear strength, since the vertical profile of drag anchors is relatively low, the change in undrained shear strength within the soil occupied by an anchor will also be low. Therefore, it has been assumed that the same yield loci can be applied to soils with undrained shear strength increasing with depth with moderate shear strength gradient.

The resistive force of the shank is assumed to have two components. The normal shank force, F_1, is calculated as the product of the shank area perpendicular to the shank, a bearing capacity factor, $N_c = 9$, and the undrained shear strength. It is assumed to act in a direction perpendicular to the shank axis and to be in a failure state. The sliding shank force, F_2, is assumed to act parallel to the shank axis and is calculated as the product of the shank surface area and the undrained shear strength. Both shank forces can be assumed to act at the shank midpoint due to the linear strength profile and constant cross-section of the shanks. The submerged weight, W_a' of the anchor is assumed to act vertically along the shank at a point midway between the shank midpoint and the fluke–shank attachment point as this is the likely centre of mass.

Equilibrium solution

The chain angle at the pad eye was calculated using an expanded form of an equation by Neubecker and Randolph (1995). The expression uses the soil strength parameters, s_{uo} and s_{ug}, the pad eye depth, d_a, the chain tension at the pad eye, T_a, the chain effective width, b_c, and a bearing capacity factor, $N_c = 9$. Ignoring the effects of chain self weight, the expanded expression becomes

$$[6] \qquad \theta_a = \left[\frac{2 b_c N_c d_a (s_{uo} + 0.5 s_{ug} d_a)}{T_a} \right]^{0.5}$$

© 2003 NRC Canada

Fig. 12. Analysis flowchart for kinematic anchor simulation using yield locus.

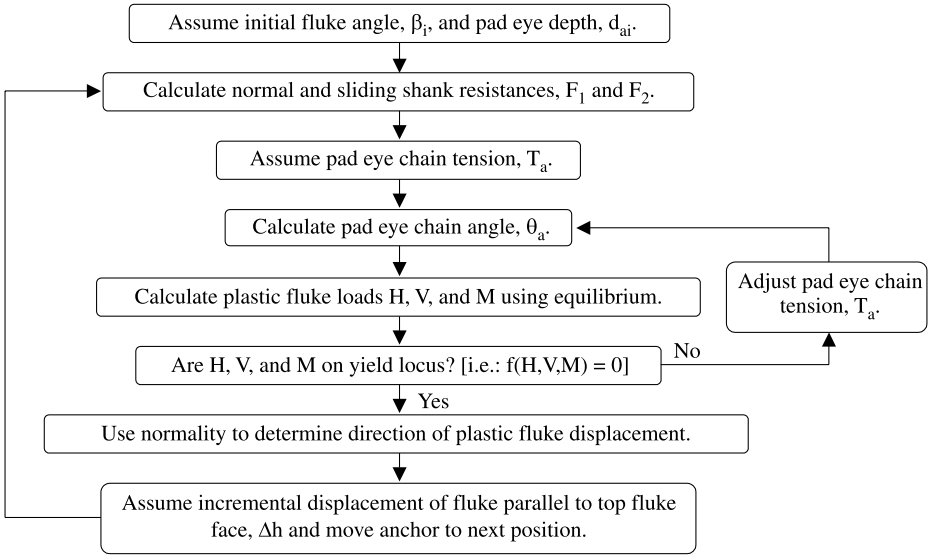

Fig. 13. Anchor-chain system for kinematic analysis.

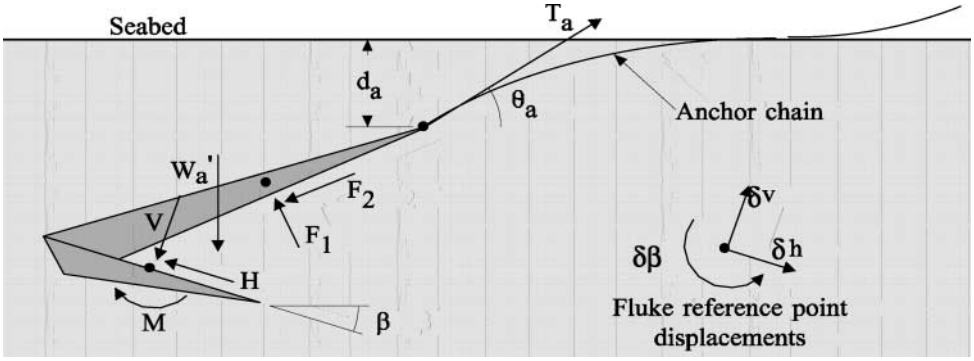

Following calculation of the shank loads, F_1 and F_2, a value of the pad eye chain tension, T_a, is assumed. Equation 6 is used to determine θ_a, after which force and moment equilibrium are applied (taking into account W_a', T_a, F_1, and F_2) to determine the fluke loads H, V, and M. A check is then performed to ensure that the fluke loads are on the plastic yield locus, such that $f(H,V,M) = 0$, and the value of T_a is adjusted and the process repeated until this requirement is satisfied.

Normality and anchor displacements

It is assumed that the shank forces have no influence on anchor kinematics, and that elastic displacements are negligible in comparison to plastic displacements. Hence, the direction of the fluke movement is governed by the normal to the plastic yield locus at the load conditions (H, V, and M) determined by the equilibrium solution

$$[7] \qquad \frac{\delta v}{\delta h} = \frac{\partial f}{\partial V} \Big/ \frac{\partial f}{\partial H}$$

and

$$[8] \qquad \frac{\delta \beta}{\delta h / L_f} = \frac{\partial f}{\partial (M/L_f)} \Big/ \frac{\partial f}{\partial H}$$

It is assumed that the fluke moves an incremental distance, Δh, in the direction parallel to the top fluke face. It follows that the incremental displacement of the fluke perpendicular to the top fluke face, Δv, is given by

$$[9] \qquad \Delta v = \left(\frac{\partial f}{\partial V} \Big/ \frac{\partial f}{\partial H} \right) \Delta h$$

and the incremental fluke rotation about the fluke reference point, $\Delta\beta$, is given by

$$[10] \qquad \Delta \beta = \left[\frac{\partial f}{\partial (M/L_f)} \Big/ \frac{\partial f}{\partial H} \right] \frac{\Delta h}{L_f}$$

Once a value of Δh is chosen, the new anchor position is updated using eqs. [9] and [10]. The analysis procedure is then restarted from the calculation of the shank loads, F_1 and F_2, until the anchor capacity T_a becomes constant and the trajectory of the anchor flattens.

Typical analysis results

Kinematic plastic yield locus analyses of a 32 tonne (t) (1 t = 1 Mg) Vryhof Stevpris anchor with a 50° shank (Vryhof Anchors 1990) are presented in this section to illus-

© 2003 NRC Canada

Table 2. Summary of parameters used in kinematic yield locus analysis of 32 t 50° Vryhof Stevpris anchor.

Property	Value
Submerged weight, W_a' (kN)	274
Shank length, L_s (m)	8.34
Shank width, b_s (m)	1.63
Fluke length, L_f (m)	4.97
Fluke width, b_f (m)	4.23
Fluke depth, d_f (m)	0.71
Fluke-shank angle, θ_{fs} (°)	41.2
Effective chain width, b_c (m)	0.24
Chain self weight, w_c (kN/m)	2.0
Surface undrained shear strength, s_{uo} (kPa)	0
Undrained shear strength gradient, s_{ug} (kPa/m)	1.5

trate the potential of the method. The anchor and soil parameters assumed in the analysis are summarized in Table 2.

The first analysis utilizes the rectangular fluke yield locus described in the section titled "Rectangular fluke analysis results", while the second analysis utilizes the wedge fluke yield locus described in the "Wedge fluke analysis results" section. The yield loci were based on eq. [5], with parameters as presented in Table 1.

Figures 14 and 15 present the results of the kinematic analysis for the 32 t Stevpris with the rectangular fluke and wedge fluke, respectively. The total drag length of each simulation was between 40 and 50 fluke lengths (or almost 250 m). Anchor efficiency, η_a is the holding force divided by the dry weight of the anchor (32 t in this case). Generally, the performance curves from both analyses are typical of drag anchor behaviour in soft clays. The anchors exhibit a steady rate of penetration into the soil early in the drag (Figs. 14*b*, 15*b*), accompanied by a sharp increase in holding capacity (Figs. 14*a*, 15*a*). With continual drag, the load and penetration curves approach plateaus at values of approximately $\eta_a = 18.9$ and $d_a = 3.2L_f$ for the rectangular fluke and $\eta_a = 18.9$ and $d_a = 3.7L_f$ for the wedge fluke, indicating that both anchors are close to their ultimate holding capacity (UHC) and full penetration (Figs. 14*a*, 14*b* and 15*a*, 15*b*). The final embedment of the wedge fluke was slightly greater than the rectangular fluke due to the different kinematic behaviour of the flukes as dictated by the respective yield loci.

Figures 14*c* and 15*c* show the chain and fluke angles during each anchor penetration. The chain angle, θ_a is equal to approximately 21°, and the fluke angle, β, is approximately 24° when the rectangular anchor has reached its ultimate capacity. The fluke angle response for the rectangular anchor in particular is interesting on two counts. Firstly, the fluke angle undergoes small but continuous oscillations during the entire simulation. The effect of these oscillations also appears in Figs. 14*a* and 14*b*. This anomaly is a result of the rectangular fluke repeatedly rotating and embedding deeper into the soil, becoming unstable due to its "blunt" tip, and rotating back to an orientation slightly shallower than before. This is exacerbated by the discontinuity of the gradient of the yield locus at $M = 0$. Secondly, the ultimate fluke angle of 24° is higher than generally observed in the field and in model tests for traditional commercial anchors with wedge-shaped flukes. This fluke angle shows that at ultimate capacity the anchor does not travel parallel to its flukes. This is also caused by the behaviour of the rectangular fluke when it travels close to parallel to its axis.

In contrast, there are no oscillations observed in the response of the wedge anchor suggesting that the "pointed" end of the wedge fluke is able to move through the soil in a stable fashion. The final fluke angle β for the wedge anchor (14°), is lower than the final fluke angle for the rectangular fluke anchor (24°). It is slightly higher than the wedge angle, $\theta_f = 9.5°$, indicating that at ultimate capacity, the anchor traveled parallel to a plane lying 4.5° outside and below the bottom fluke face (Fig. 15*c*). This is in reasonable agreement with the experimental results obtained from 1*g* and centrifuge tests using the 1:80 scale model Vryhof Stevpris anchor in clay (O'Neill 2000), as well as the results of published field and scale model tests where it was found that the anchor moved along a direction within the edge, but close to the bottom face. The final chain angle, $\theta_a = 24°$ is slightly higher than the value of 21° calculated for the rectangular fluke anchor. This is due to the shallower final fluke angle, which orientates the fluke so that it makes a larger component of its *V* resistance available to act against the vertical component of chain force at the pad eye, resulting in an increase in θ_a.

The plastic failure loads *H*, *V*, and *M* acting on the rectangular and wedge flukes are also plotted against the normalized horizontal drag length in Figs. 14*d* and 15*d*. The loads are normalized with respect to their maximum and offset values (e.g., the load *H* is presented as $(H - H_1)/(H_{max} - H_1)$). For the rectangular fluke when H_1, M_1, $V_1 = 0$ this is equivalent to plotting H/H_{max}, $M/M_{max,}$ and V/V_{max}. As the drag of the rectangular wedge anchor proceeds, the normalized horizontal fluke load decreases somewhat, while the normalized vertical load increases (Fig. 14*d*). The normalized moment acting on the fluke also decreases. The plot further illustrates the oscillating behaviour of the anchor, even as it reaches a "stable" UHC and embedment depth. The average final normalized *H*, *V*, and *M* values were 0.77, 0.82, and 0.00, respectively. The high *H* value is unsurprising since the displacement of the fluke is predominately in (or close to) the direction parallel to the fluke face (*h*). The normalized *M* value of zero is also expected, since at UHC the anchor orientation is stable ($\delta\beta = 0$), and therefore $M = M_1$. The final *V* value was slightly higher than predicted, and can be explained by the fact that β was greater than expected at UHC. This implies that the anchor was not traveling parallel to the fluke face, and so there was a component of movement perpendicular to this, thereby mobilizing vertical load onto the fluke. The load sharing of the anchor with the wedge-shaped fluke is quite similar but without the instabilities (Fig. 15*d*). The horizontal load dropped slightly over the course of the drag, from an initial normalized value of 0.98 to an ultimate value of 0.82. The normalized moment also decreased, from 0.08 to 0.00, while the normalized vertical load increased from 0.40 to 0.75.

Figures 14*e* and 15*e* show the load paths undergone by each fluke over the entire drag. The loads are normalized with respect to their maximum and offset values. In each load space plot, the yield locus is shown with the third load dimension equal to the related offset value (for example in the *V*-*H* plot, $M = M_1$ on the yield locus). The arrow in each

© 2003 NRC Canada

Fig. 14. Kinematic analysis for 32 t 50° Vryhof Stevpris using rectangular fluke yield locus.

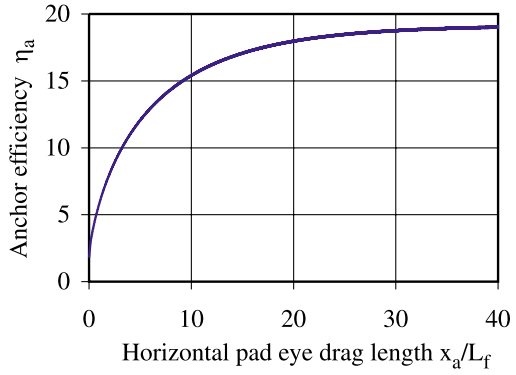

(a) Anchor capacity

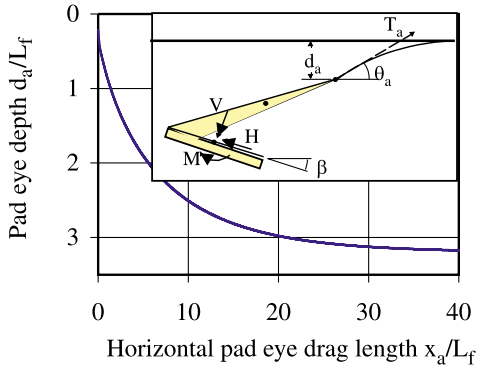

(b) Anchor trajectory

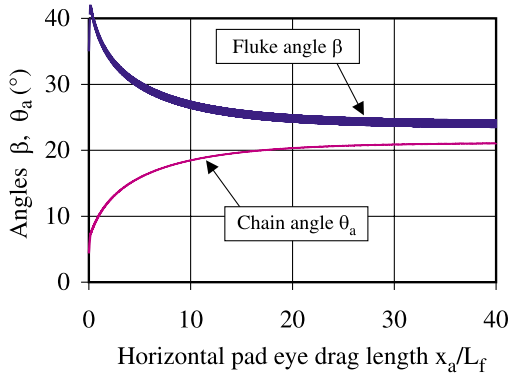

(c) Fluke and chain angles

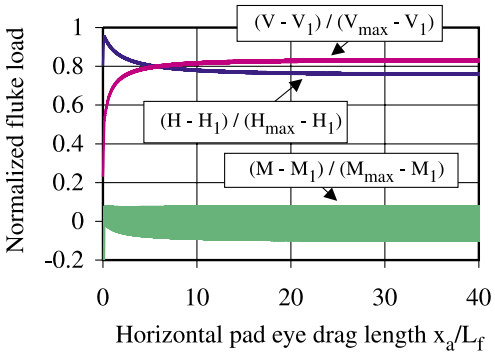

(d) Fluke load components

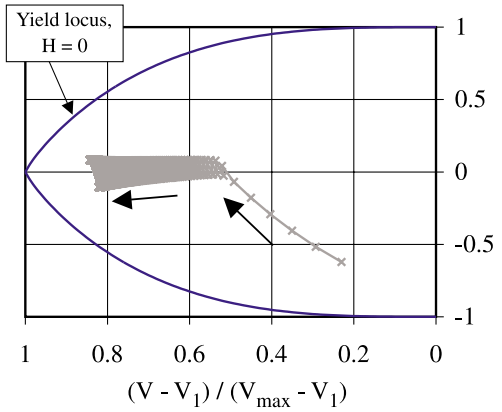

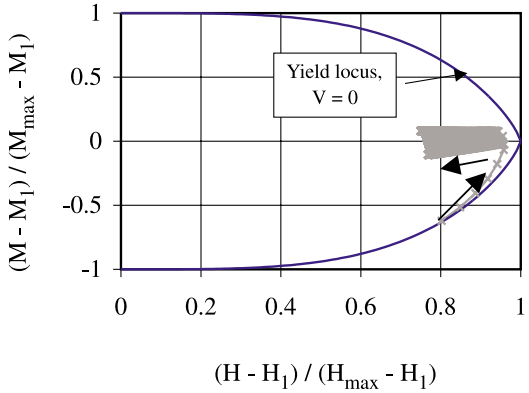

(e) Fluke load in H-V-M load space

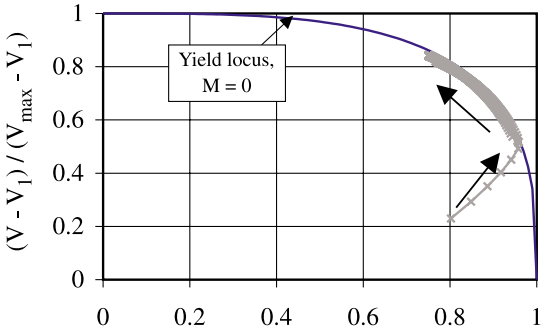

© 2003 NRC Canada

Fig. 15. Kinematic analysis for 32 t 50° Vryhof Stevpris using wedge fluke yield locus.

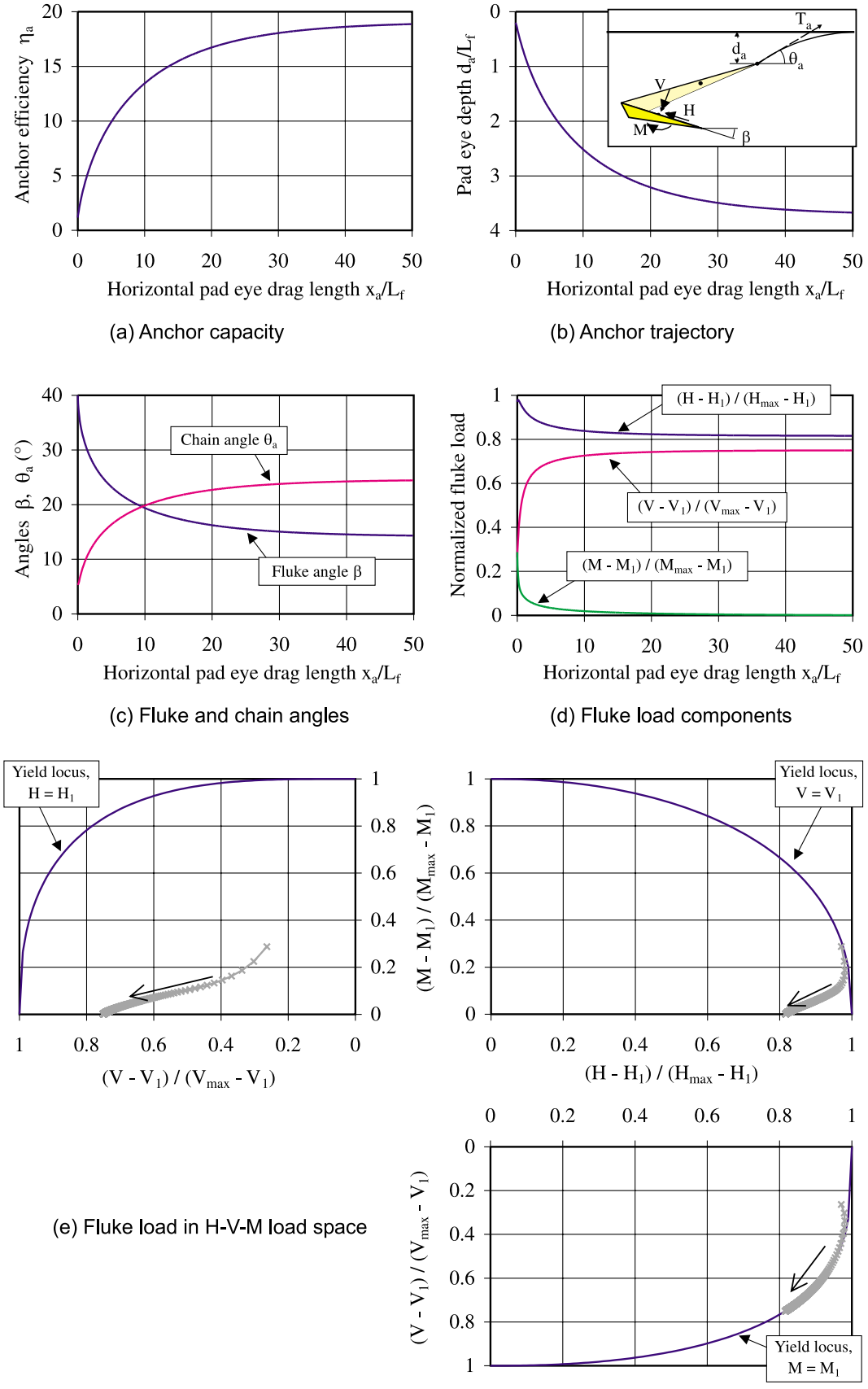

© 2003 NRC Canada

Fig. 16. Comparison of kinematic wedge fluke yield locus model with Neubecker–Randolph model (Neubecker and Randolph 1996) for 32 t 50° Vryhof Stevpris.

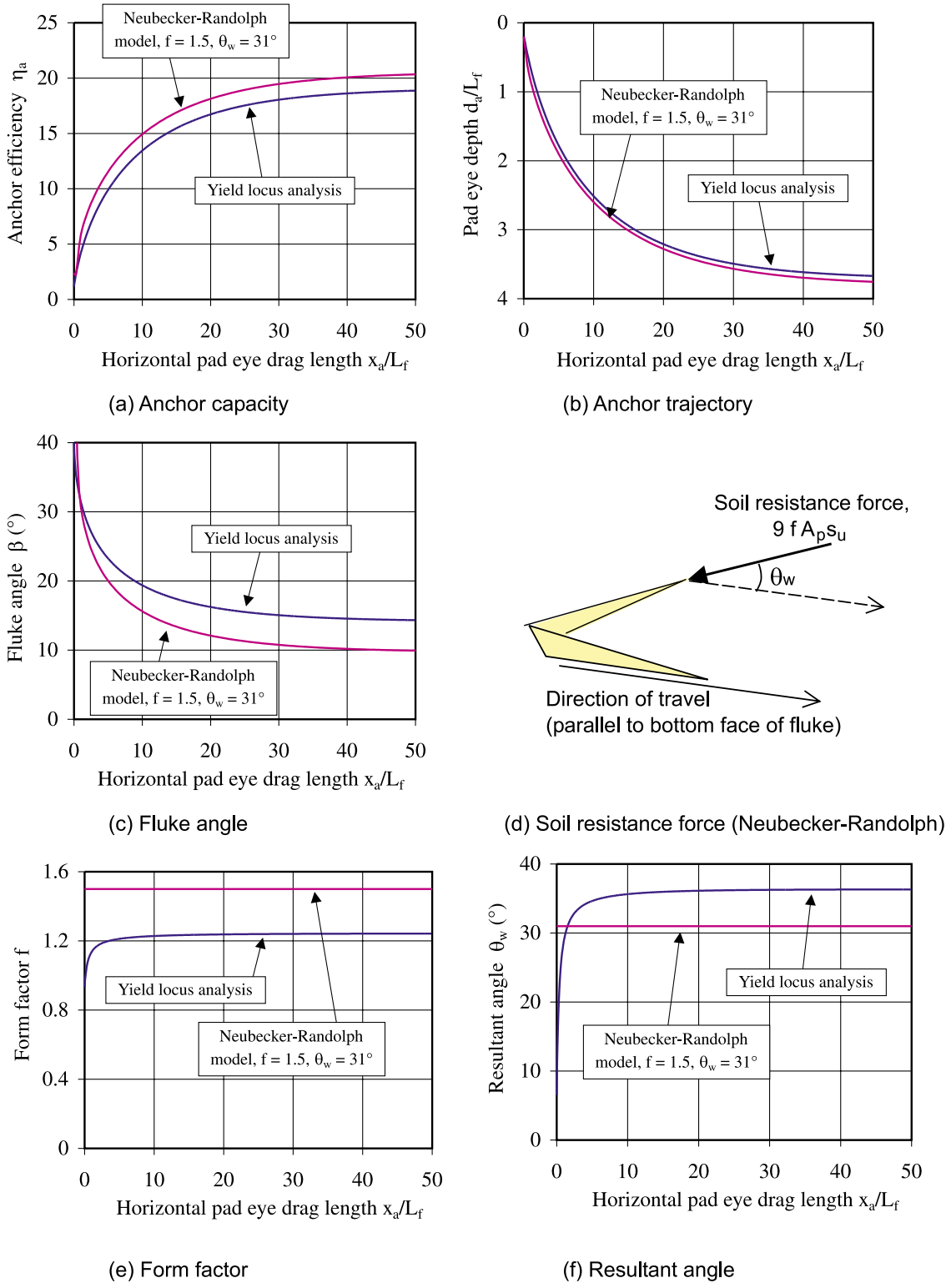

subplot indicates the direction of the load change as the drag proceeded. For both anchors, the fluke load path remains on the 3D plastic yield locus, despite the 2D representation suggesting that they drift off the plastic yield locus because the third load component was not always equal to the reference value. Since M quickly fell towards M_1, the load path in H-V space tracked very close to the $M = M_1$ yield locus until it stabilized so that the plastic normal gave $\delta v/\delta h = \tan\beta_{uhc}$.

© 2003 NRC Canada

Comparison with anchor design charts and methods

Figure 16 shows a comparison between the standard wedge fluke yield locus analysis of the 32 t 50° Vryhof Stevpris, featured in Fig. 15, and the predicted performance for the same anchor and soil conditions as calculated using the Neubecker–Randolph incremental simulation procedure (Neubecker and Randolph 1996). The Neubecker–Randolph simulation quantifies anchor resistance parallel to the upper fluke face as $fA_pN_cs_u$, where f is a form factor, A_p is the projected area of the anchor and N_c is a bearing capacity factor (taken as 9). They also assume that the resultant resistance acts at an angle, θ_w, to the fluke face. Curves in Fig. 16 have been obtained with f = 1.50 and θ_w = 31.0°, selected to match data from 1:80 scale model tests of a 32 t 50° Stevpris anchor in clay (O'Neill 2000). The anchor efficiencies from the two methods are in reasonable agreement (Fig. 16*a*), with the Neubecker–Randolph simulation, suggesting a final η_a = 20.3 after 50 fluke-lengths of drag (approximately 8% higher than from the yield locus method). Likewise, the pad eye embedment trajectory (Fig. 16*b*) compares very well with the Neubecker–Randolph simulation, predicting a final $d_a = 3.76L_f$, which is only 2% greater than the result from the yield locus analysis method. The fluke angle curve obtained from the Neubecker–Randolph simulation (Fig. 16*c*) was calculated assuming that the fluke travels parallel to its bottom face, but the simulation suggests that the anchor travels at 4° below the bottom face of the anchor at its UHC.

Figures 16*e* and 16*f* also present the values of the form factor, f, and resultant angle, θ_w, as calculated from the results of the wedge fluke yield locus analysis for the 32 t Stevpris anchor. The yield locus method suggests that f = 1.24 towards UHC, which is lower than the experimentally derived value, f = 1.50. Furthermore, the yield locus θ_w value of 36.3° is higher than the value of 31.0° calculated for the 1:80 scale model. Hence, there are differences in the contribution of the fluke to the anchor capacity using the two methods. However, considering the simplifications made in the yield locus model and the assumption of the geotechnical forces in the Neubecker–Randolph model, this reasonable comparison suggests that the yield locus approach to the analysis and design of drag anchors is promising.

Predictions of anchor holding capacity, T_a, against dry anchor weight, W_a, for the 50° Vryhof Stevpris determined using the wedge fluke yield locus model, Vryhof Anchors (1990), the NCEL (1987), the IFP (Le Tirant and Meunier 1990), and the Neubecker–Randolph model tests (Neubecker and Randolph 1996; using average f and θ_w values calculated for the tests by O'Neill 2000) are shown in Fig. 17*a*. The yield locus and Neubecker–Randolph curves were calculated assuming zero undrained shear strength at the surface, and an undrained shear strength gradient, s_{ug} = 1.5 kPa/m. The remainder of the curves were obtained from the results of full-scale trials in "soft clay". The yield locus curve matches the Neubecker–Randolph curve very well. Both curves predict more anchor capacity than the NCEL and IFP curves, but less capacity than the Vryhof curve. Fluke tip depth, d_t at UHC versus W_a is presented in Fig. 17*b*, and again the new results lie parallel to and just below the Neubecker–Randolph curve. In comparison, both the Vryhof and NCEL curves suggest that there is less embedment achieved for the small and midsized anchors compared to the theoretical predictions.

Fig. 17. Comparison of anchor design charts and methods with kinematic wedge fluke yield locus model for Vryhof Stevpris in soft clay (data from NCEL 1987; Vryhof Anchors 1990; Le Tirant and Meunier 1990; Neubecker and Randolph 1996).

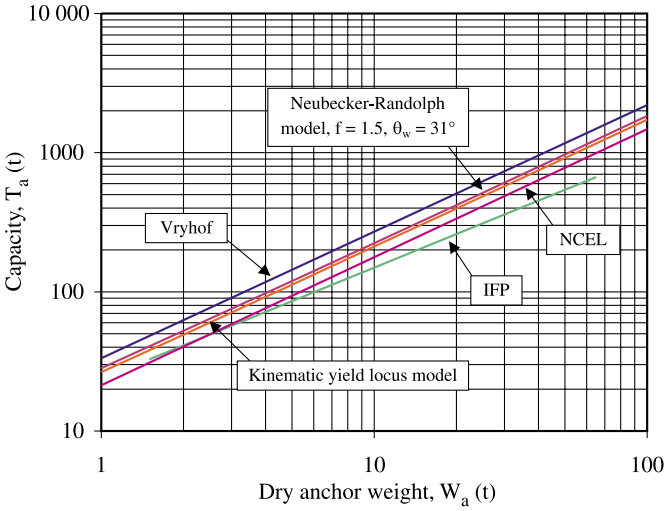

(a) Holding capacity, T_a

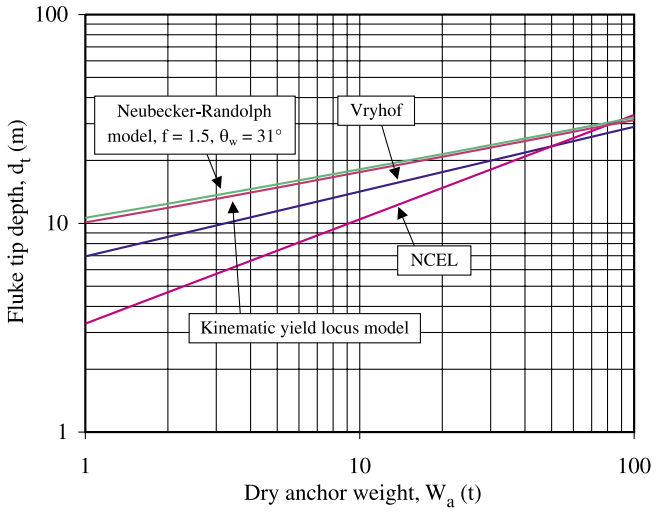

(b) Fluke tip depth, d_t

Conclusions

Two-dimensional FE analysis has been used to examine both the local failure mechanisms governing the development of holding capacity and the kinematics of simplified drag anchor flukes. In turn, the observed plastic failure behaviour has been characterized with yield loci, expressed in terms of moment and loads parallel and normal to the fluke.

© 2003 NRC Canada

The two fluke geometries explored have been shown to result in slightly different yield loci as a result of different failure mechanisms, particularly under horizontal loading. Mathematical expressions fitted to the data provide idealized yield loci in combined load space, as well as plastic potentials enabling calculation of the incremental fluke displacement directions. These loci have been implemented into a new analytical design procedure for the prediction of drag anchor behaviour in soft clays. Despite the simplifications adopted in the analysis, results from the procedure have been shown to compare well with experimental and field test data. This suggests that the approach has promise, and with further refinement of the yield loci and better approximations to the complex anchor geometry, it may develop into a useful anchor design tool.

Acknowledgements

The work described in this paper forms part of the activities of the Special Research Centre for Offshore Foundation Systems, established and supported under the Australian Research Council's Research Centres Program.

References

Baligh, M.M., and Scott, R.F. 1976. Analysis of wedge penetration in clay. Géotechnique, **26**(1): 185–208.

Bransby, M.F., and Randolph, M.F. 1997. Shallow foundations subject to combined loadings. *In* Proceedings of the 9th International Conference on Computer Methods and Advances in Geomechanics. Wuhan, November. *Edited by* J. Yuan. A.A. Balkema, Rotterdam. Vol. 3, pp. 1947–1952.

Bransby, M.F., and Randolph, M.F. 1998. Combined loading of skirted foundations. Géotechnique, **48**(5): 637–655.

Britto, A., and Gunn, M. 1987. Critical state soil mechanics via finite element analysis. Ellis Horwood Ltd., Chichester.

Chen, W.F. 1975. Limit analysis and soil plasticity, Elsevier, N.Y.

Colwill, R.D. 1996. Marine drag anchor behaviour — a centrifuge modelling and theoretical investigation. Ph.D. thesis, The University of Manchester, Manchester, U.K.

Dahlberg, R. 1998. Design procedures for deepwater anchors in clay. *In* Proceedings of the 30th Offshore Technology Conference. Houston, Tex. OTC 8837.

Le Tirant, P., and Meunier, J. 1990. Anchoring of floating structures. Editions Technip, Paris, France.

Martin, C.M. 1994. Physical and numerical modelling of offshore foundations under combined loads. Ph.D. thesis, University of Oxford, U.K.

Martin, C.M., and Houlsby, G.T. 2001. Combined loading of spudcan foundations on clay: numerical modelling. Géotechnique, **51**(8): 687–699.

Merifield, R., Sloan, S., and Yu, H. 2001. Stability of plate anchors in undrained clay. Géotechnique, **51**(2): 141–153.

Murff, J.D. 1994. Limit analysis of multi-footing foundation systems. *In* Proceedings of the 8th International Conference on Computer Methods and Advances in Geomechanics. Morgantown, May. *Edited by* H.J. Siriwardane and M.M. Zaman. A.A. Balkema, Rotterdam. Vol. 1, pp. 223–244.

Naval Civil Engineering Laboratory (NCEL). 1987. Drag embedment anchors for navy moorings. Naval Civil Engineering Laboratory, Port Hueneme, Calif., Techdata Sheet 83–08R.

Neubecker, S.R., and Randolph, M.F. 1995. Profile and frictional capacity of embedded anchor chain. Journal of the Geotechnical Engineering Division, ASCE, **121**(11): 787–803.

Neubecker, S.R., and Randolph, M.F. 1996. The performance of drag anchor and chain systems in cohesive soil. Marine Georesources and Geotechnology, **14**: 77–96.

O'Neill, M.P. 2000 The behaviour of drag anchors in layered soils. Ph.D. thesis, The University of Western Australia, Crawley WA, Australia.

Rowe, R.K., and Davis, E.H. 1982. The behaviour of anchor plates in clay. Géotechnique, **32**(1): 9–23.

Sloan, S.W., and Randolph, M.F. 1982. Numerical prediction of collapse loads using finite element methods. International Journal for Numerical and Analytical Methods in Geomechanics, **6**(6): 47–76.

Tan, F. 1990. Centrifuge and theoretical modelling of conical footings on sand. Ph.D. thesis, The University of Cambridge, Cambridge, U.K.

Thorne, C.P. 1998. Penetration and load capacity of marine drag anchors in soft clay. Journal of Geotechnical and Geoenvironmental Engineering, **124**(10): 945–953.

Vryhof Anchors 1990. Anchor manual. Krimpen ad Yssel, The Netherlands.

List of symbols

A_p	projected area of the anchor
b_c	effective width of chain
b_f	fluke width
b_s	shank width
d_a	anchor pad eye embedment depth
d_{ai}	initial anchor embedment depth
d_f	depth/thickness of fluke
f	yield locus function
f	form factor (Neubecker and Randolph 1996)
F_1, F_2	normal and sliding shank resistances, respectively
G	shear modulus of soil
δh	displacement component parallel to fluke top face
H	load component parallel to fluke top face
H_1	offset H load for curve-fitting (H when $\delta h = 0$)
H_{max}	maximum load capacity parallel to fluke top face
L_f	length of fluke
L_s	shank length
m, n,	
q, p	failure locus curve fitting factors
M	moment applied about fluke reference point
M_{max}	maximum moment able to be sustained by the fluke
M_1	offset M load for curve-fitting (M when $\delta\theta = 0$)
N_c	shank bearing capacity factor
s_f	displacement of fluke $(\delta v^2 + \delta h^2)^{0.5}$
s_u	undrained shear strength of soil
s_{ug}	undrained shear strength gradient
s_{uo}	undrained shear strength of soil immediately at seabed ($z = 0$)
T_a	chain tension at the pad eye
δv	displacement component perpendicular to fluke top face
V	load component perpendicular to fluke top face
V_1	offset V load for curve-fitting (V when $\delta v = 0$)
V_{max}	load capacity perpendicular to fluke top face
w_c	chain self-weight
W_a	dry anchor weight
W_a'	submerged weight of anchor

© 2003 NRC Canada

x_a padeye drag length
z depth below seabed
α geometrical variable in upper bound mechanisms
β angle of inclination of top face of fluke
$\delta\beta$ rotation of fluke
β_i initial inclination of fluke
β_{uhc} inclination of fluke at ultimate holding capacity
η_a anchor efficiency (holding force/dry weight)
θ_a chain inclination to horizontal at the pad eye
θ_f fluke-wedge angle
θ_{fs} fluke-shank angle
θ_w resultant angle (Neubecker and Randolph 1996)
ν Poisson's ratio

© 2003 NRC Canada